Numerical Heat Transfer, Part A, 49: 655–667, 2006

ISSN: 1040-7782 print/1521-0634 online
DOI: 10.1080/10407780500343798

Taylor & Francis
Taylor & Francis Group

NATURAL CONVECTION IN AN ENCLOSURE WITH DISTRIBUTED HEAT SOURCES

A. Bazylak, N. Djilali, and D. Sinton
Institute for Integrated Energy Systems and Department of Mechanical Engineering, University of Victoria, Victoria, BC, Canada

Presented in this article is a computational analysis of the heat transfer due to an array of distributed heat sources on the bottom wall of a horizontal enclosure. The heat sources are modeled as flush-mounted sources with prescribed heat flux boundary conditions. Optimum heat transfer rates and the onset of thermal instability triggering various regimes are found to be governed by the length and spacing of the sources and the width-to-height aspect ratio of the enclosure. With respect to source spacing, we found that spacing equal to that of the source length provides effective convective heat transfer, and increasing the source spacing further does not result in significant improvements. The transition from a conduction-dominated regime to a convection-dominated regime is found to be characterized by a range of Rayleigh numbers, in contrast to the classical bottom wall heating problem. The range of Rayleigh numbers at which transition takes place decreases as the source length increases. At the transition region for very small source lengths, the Rayleigh-Bénard cell structure grows significantly to form fewer and larger cells, which accounts for higher heat transfer rates compared to configurations with longer heat sources where the cell structure remains the same throughout transition. Following the transition to a convection-dominated regime, bifurcations in the Rayleigh-Bénard cell structures as well as further regime changes are observed, reflecting the instabilities in the physical system.

INTRODUCTION

This work is motivated by the need for passive cooling through natural convection in the area of microelectronic devices, where increasing dissipative heat flux and increasing component density demand more efficient heat removal. The low thermal conductivity of commonly used organic materials intensifies the impact of this high heat flux by causing large temperature gradients between components and their substrate [1]. Finned, air-cooled heat sinks and liquid cooling are alternative designs for heat removal, but the major drawbacks of these designs are the increases in weight, cost, and volume [1]. Natural convection provides a means to facilitate and enhance

Received 15 April 2005; accepted 18 August 2005.
The authors are grateful for the financial support of the Natural Sciences and Engineering Research Council (NSERC) of Canada, through a postgraduate scholarship to A. Bazylak and research grants to N. Djilali and D. Sinton. Financial support from the University of Victoria, through a postgraduate scholarship to A. Bazylak, is also gratefully acknowledged.
Address correspondence to N. Djilali, University of Victoria, Department of Mechanical Engineering, P.O. Box 3055 STN CSC, Victoria, BC V8W 3P6, Canada. E-mail: ndjilali@uvic.ca

NOMENCLATURE

C_p	specific heat capacity	S	length of spacing between sources
$\vec{g}$	Acceleration of gravity	t	time
h	heat transfer coefficient	T	temperature
	$(= q''_L/T_S - T_L)$	T_L	top wall temperature
H	height of plenum	$T_{\max}$	maximum temperature of heat source
k	thermal conductivity		surface
L	length of heat source	$\vec{v}$	velocity
Nu	Nusselt number	α	thermal diffusivity of air
P	static pressure	β	thermal expansion coefficient
Pr	Prandtl number	ΔT	difference between local temperature
q''_L	source heat flux		and top wall temperature $(= T - T_L)$
q''_S	spacing heat flux	ν	kinematic viscosity of air
Ra	Rayleigh number	ρ	fluid density

heat and mass transfer for microelectronic devices. Natural convection is also an area of interest for enhanced heat and mass transfer for recently developed biochemical analysis systems and micro-fuel cell designs [2–4]. The purpose of this article is to study the effects of an infinite array of distributed heat sources in a horizontal air-filled plenum. Rayleigh numbers ranging from 0.1 to 10,000 are of interest, corresponding to dry air temperature differences from 10°C to 160°C and characteristic lengths ranging from 500 μm to 10 mm.

Numerous studies have been performed on horizontal fluid layers heated from below [5–9]. A growing body of work also exists in the area of convection due to discrete heat sources because of its fundamental interest and relevance to applications in electronics [10–21]. Incropera et al. [10] performed experiments to determine the heat transfer due to conduction and forced convection from a four-row array of 12 heat sources flush-mounted on one wall of a horizontal channel filled with water. Heindel et al. [11, 12] studied the natural convection from an array of discrete heat sources in a cavity filled with water and a dielectric fluid. They also investigated the natural-convection heat transfer for an array of finned, discrete heat sources in a cavity filled with a dielectric fluid [13]. Ortega and Lall [14] performed experiments to measure the heat transfer coefficient on the surface of a square flush-mounted heat source at the center of a plate in a small horizontal enclosure. Deng et al. [15] presented a two-dimensional numerical investigation of natural convection from two discrete flush-mounted heat sources in a horizontal enclosure with insulating side walls at steady state to investigate the interaction between sources. Tou and Zhang [16] presented a three-dimensional numerical model to investigate the heat transport in a liquid-filled vertical rectangular enclosure with a 3×3 array of discrete flush-mounted heaters along one vertical wall. The opposite wall acted as a uniform cold surface, and all other walls were insulting. Bae and Hyun [17] studied two-dimensional laminar natural-convective air cooling in a vertical rectangular enclosure with three discrete flush mounted heaters on one side of the wall. The thermal condition of the lowest-elevation heater alternated between ''on'' and ''off,'' and the resulting effect on transient heat transfer for the other sources was studied. Da Silva et al. [18] investigated the optimum distribution of heat sources cooled

by laminar natural convection for a small number of heat sources mounted on the side wall of an enclosure and for a large number of heat sources mounted on a vertical wall facing a fluid reservoir. Da Silva et al. [19] also investigated the optimal distribution and sizes of three discrete heat sources in a vertical open channel cooled by natural convection. Tso et al. [20] presented experimental and numerical results for laminar natural-convection cooling of water in a rectangular cavity with a 3×3 array of heaters on one wall at various angles of inclination. Papanicolaou and Gopalakrishna [21] presented a two-dimensional computational investigation of natural convection in a shallow horizontal air layer driven by a single flush-mounted, discrete, constant heat flux source. They investigated the parameters governing the transition from the conduction-dominated regime to a convection-dominated regime. The geometric parameters studied in their work are the width-to-height aspect ratio of the air layer to the uniformly heated source size. With a uniform heat source, a discrete transition region was observed, whereas with discrete heating, the transition was continuous. For each source size, an optimum aspect ratio for heat transfer was found. In the presence of three discrete heat sources, they found that the transition from conduction to convection was significantly delayed in the presence of adjacent sources compared to the single source; however, the rate of increase of Nusselt number with increasing Rayleigh number was higher in the case of multiple heat sources.

The design of more efficient passive cooling for high-density packaging of electronic devices requires a better understanding of the parameters governing natural-convective heat transfer in the basic arrangement of a horizontal enclosure with many discrete heat sources. This work provides new insight on the physical parameters, such as source length and spacing, which control the onset and generation of sustained natural convection in a horizontal air layer with a large number of heat-generating components. Specifically, the limiting case of an infinite array of distributed heat sources is simulated with the use of periodic boundary conditions. We determine the effects of source spacing and source lengths on heat transfer rates and flow regimes, and we discuss the impact of using periodic boundary conditions in modeling these flows.

MATHEMATICAL MODEL

Figure 1 llustrates the geometric and thermal boundary conditions of the two-dimensional problem under consideration. Temperature contours for the conduction-dominated regime for this configuration are also shown in Figure 1. Flush-mounted heat sources of equal length, L, have prescribed heat flux boundary

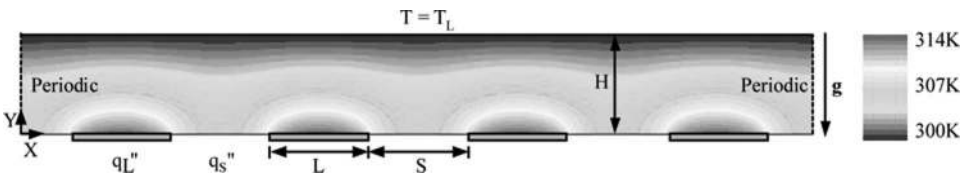

Figure 1. Schematic of computational domain showing geometric and thermal boundary conditions with temperature contours plotted for a conduction-dominated regime (Ra = 0.2).

conditions, q''_L. The heat sources are separated by length, S, and the height of the plenum is H.

The following conditions are prescribed on the other boundaries.

Bottom wall, between sources: zero heat flux boundary condition, $q''_S = 0$
Top wall: constant temperature, T_L
Bottom and top walls: no-slip velocity conditions
Side boundaries: periodic boundary condition

The periodicity condition simulates a wide array of heat sources with no influence from side walls. Having a sufficiently large computational domain between periodic boundary conditions is of critical importance to the numerical results in order to avoid constraining the wavelength of the convection patterns. In some cases, the computational domain size requirements change with the regime, as will be discussed later. In this work, the maximum temperature difference ΔT is assumed to be small enough to justify the use of the Boussinesq approximation, and the continuity, momentum, and energy equations governing the flow and heat transfer are given by

$$\nabla \cdot \vec{v} = 0 \tag{1}$$

$$\frac{\partial \vec{v}}{\partial t} + \nabla \cdot (\vec{v}\vec{v}) = -\frac{1}{\rho}\nabla P + \nu \nabla^2 \vec{v} + \beta \Delta T \vec{g} \tag{2}$$

where, $\vec{v}$ is the velocity vector, t is the time, ρ is the fluid density, P is the static pressure, ν is the kinematic viscosity, β is the thermal expansion coefficient, and $\vec{g}$ is the acceleration of gravity.

$$\rho C_p \left(\frac{\partial T}{\partial t} + \vec{v} \cdot \nabla T \right) = k \nabla^2 T \tag{3}$$

where C_p is the specific heat capacity, k is the thermal conductivity, and T is the temperature.

The heat transfer from the sources is expressed in terms of the Nusselt number averaged over the area of the source, which is defined as

$$\mathrm{Nu} = \frac{hH}{k} \tag{4}$$

where h is the heat transfer coefficient, and H is the characteristic length of the system. There are several length parameters associated with this geometry, such as the plenum height, H, heat source length, L, and spacing length, S. The characteristic length of the system is defined here as the plenum height, H, which greatly impacts the Rayleigh-Bénard cell structure and pattern. The Rayleigh number is defined as

$$\mathrm{Ra} = \frac{g\beta(T_{\max} - T_L)H^3}{\alpha\nu} \tag{5}$$

where T_{max} is the maximum temperature on the surface of heat source and α is the thermal diffusivity of air. The Rayleigh number is calculated *a posteriori* once T_{max} has been determined from the simulations. For evenly spaced distributed heat sources, the ratio of source length to height (L/H) is also an important parameter. For materials with low emissivity, radiation is not a significant heat transfer mechanism and is neglected throughout this investigation. The Prandtl number has a value of 0.74 and is given by

$$\mathrm{Pr} = \frac{\nu}{\alpha} \tag{6}$$

This model was implemented in Fluent, a commercial finite-volume-based computational fluid dynamics (CFD) package. The governing equations and the prescribed boundary conditions were discretized with a QUICK scheme [22], and PRESTO was used as the descretization method for pressure [22]. The SIMPLE method was used for the pressure–velocity coupling scheme, and a slightly stretched hexagonal grid and a segregated solver were used for all simulations.

RESULTS AND DISCUSSION

In an infinite horizontal layer being heated from below, the theoretical critical Rayleigh number is 1,708 [23]. Soong et al. [8] found that the presence of confining side walls results in a higher critical Rayleigh number, and Papanicolaou and Gopalakrishna [21] reported that for a discrete heat source with confining side walls, there is a range of critical Rayleigh numbers, depending on the length of the source and the height of the domain. In this article, the constraint of the side walls is removed, effectively considering an infinite array of distributed heat sources and their effects on heat transfer. Along with the trend of increasing electronic miniaturization, there is also a trend toward increasing component density. As the number of electronic components increases and plenum height decreases, the end effects become much less significant, and the spacing between the components becomes the dominant parameter. The geometry and periodicity considered here are thus good representations of such conditions.

Source Spacing

The effect of source spacing was investigated with the geometry shown in Figure 1 at steady state with uniform and equal heat flux boundary conditions for each heat source. The effects of varying the spacing between sources on heat transfer and maximum velocity are presented in Figure 2; the source length, L, and plenum height, H, are equivalent ($L = H$), and this one-to-one ratio is held constant. The Rayleigh number is increased to study the effects on the average Nusselt number when the dimensionless spacing length between the sources, S/L, is varied.

Figure 2*a* shows that the Nusselt number begins to plateau for $S/L > 1$. Rayleigh numbers range from 730 to 890 in the convection-dominated regime, and from 45 to 75 in the conduction-dominated regime. Heat transfer is not maximized for shorter spacing lengths, and there are no dramatic benefits to increasing the

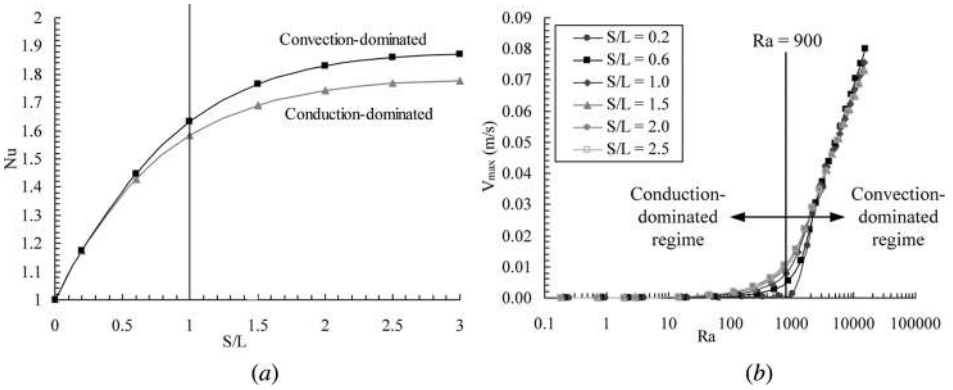

Figure 2. Effect of varying spacing between heat sources on (*a*) heat transfer and (*b*) maximum velocity.

spacing length further. It is also noteworthy that longer separation lengths are not desirable in the applications of interest. Figure 2*b* shows the maximum velocity versus Rayleigh number for different source spacings. The transition from the conduction-dominated regime to the convection-dominated regime occurs at $\mathrm{Ra} = 900$, and the rate at which the maximum velocity increases with increasing Ra also reaches a ceiling for spacing lengths larger than $S/L = 1$. Papanicolaou and Gopalakrishna [21] used a spacing of 0.5 times the length of the source to ensure significant interaction among three heat sources. Results from our investigation bring new insight on an improved heat source distribution pattern that enhances heat transfer for large numbers of sources. Considering the results shown in Figure 2 and the simplicity of the $S = L$ configuration, this source pattern is utilized in all following computations.

Figure 3 shows typical temperature and convection patterns in the convection-dominated regime for the horizontal fluid layer heated from below by distributed heat sources where $S = L = H$. The temperature contours in Figure 3*a* show the thermal plumes that develop above each heat source. The velocity streamfunctions shown in Figure 3*b* show the development of Rayleigh-Bénard convection cell pairs above each heat source. Figures 3*c* and 3*d* show the velocity vectors associated with the cell structures. Buoyancy forces induce the heated fluid at the source to rise vertically toward the upper cooled surface. The temperature of the fluid cools as it reaches the upper surface and is driven downward, where its temperature begins to rise again due to the heat source. The $S = L = H$ configuration leads to the stable repeating pattern of roughly circular circulations centered on the edges of each source.

Source Length

In the following simulations, the source length and the spacing length are equal ($S = L$), and this ratio is kept constant as the Rayleigh number is increased. The average Nusselt number versus Rayleigh number is plotted in Figure 4 for various ratios of source length to plenum height, L/H. Figure 4 shows the effect on heat transfer when increasing the length of the heat sources. In agreement with [21], the transition

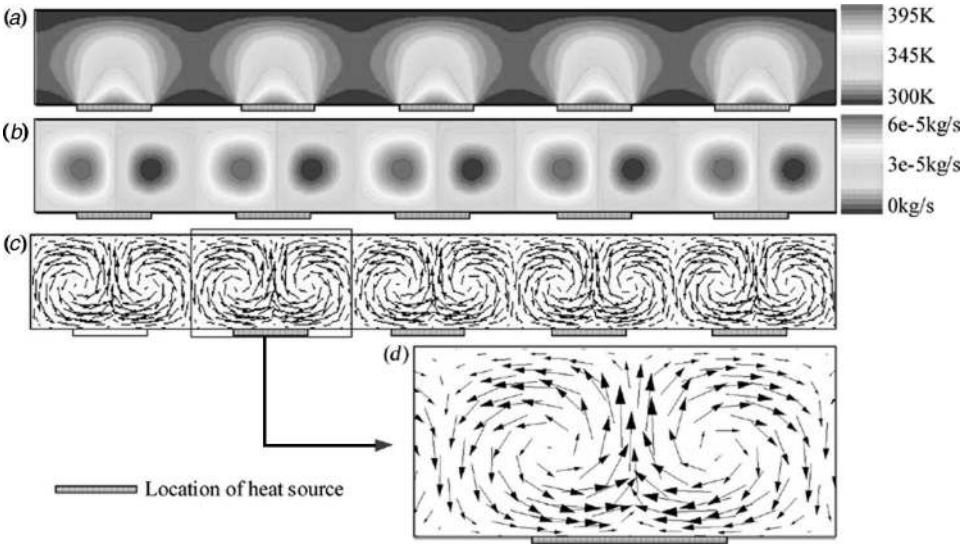

Figure 3. Distributed heat sources with uniform heat flux boundary conditions where $S = L = H$ and Ra = 1,350: (*a*) temperature contours; (*b*) velocity streamfunctions; (*c*) velocity vectors; (*d*) velocity vectors surrounding each heat source.

from a conduction-dominated regime to a convection-dominated regime occurs in the elbow region of the average Nu versus Ra plot, at Ra $\approx$ 1,000. Papanicolaou and Gopalakrishna [21] found that with three discrete heat sources, flow transitioned to the convection-dominated regime above the middle source at Ra = 2,347 and above the side sources at Ra = 1,509. The flow above the side sources experienced a relatively earlier transition due to the effects of confining side walls. In our work, the transition region occurs at Rayleigh numbers ranging from 500 to 2,000, for source lengths ranging from $L = 0.1\,H$ to $L = 1.8\,H$, and the transition occurs at the same Rayleigh number for all sources since there are no confining side walls. As the length

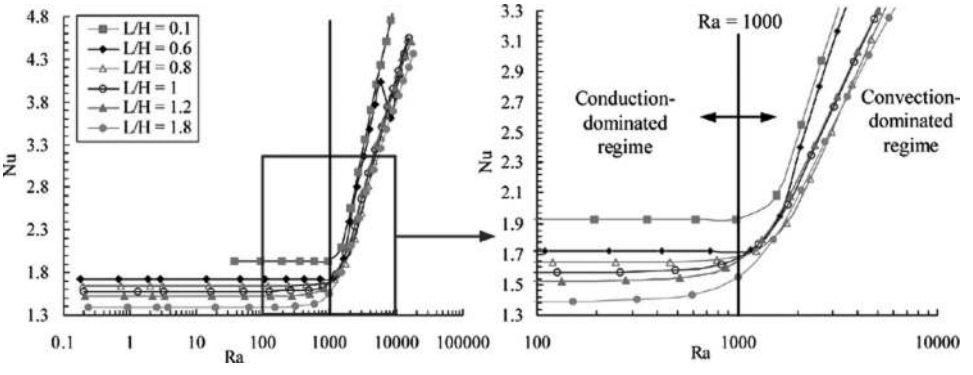

Figure 4. Average Nusselt number versus Rayleigh number for various source lengths, L, while keeping the source spacing and source length equivalent ($S = L$).

of the heat source element increases, the transition begins at smaller Rayleigh numbers and grows slowly with Rayleigh number. As the length of the heat source element decreases, the heat flux becomes more evenly distributed, and the solution approaches that of the classical bottom wall heating configuration, which exhibits a sharper transition region as reported in [21]. In the conduction-dominated regime, the average Nusselt number decreases as the source length relative to the plenum height increases. The rate of increase of the average Nu decreases as the source length increases in the convection-dominated regime. In the convection-dominated regime, Nu increases steadily with Ra, with the $L = 0.1\,H$ source length configuration showing the best rate of heat transfer. The $L = 0.6\,H$ shows an irregularity between Rayleigh numbers 5,800 to 8,100, which will be revisited later.

Figure 5 shows the maximum velocity versus Ra for various source lengths and, similar to the curves shown in Figure 4, the transition region occurs where $\mathrm{Ra} \approx 1{,}000$. The maximum velocity increases at a faster rate as Ra increases for longer sources. In Figure 5, a higher maximum velocity occurs in the transition region for increasing source lengths. In the convection-dominated regime well beyond the transition region, the maximum velocities for varying source lengths approach the same values and increase at the same rate.

For the cases with relatively small source lengths, the Rayleigh-Bénard cells undergo significant growth in the transition region. For the source length of $L = 0.1\,H$, pairs of weak convection cells are observed over each heat source in the conduction-dominated regime, as shown in Figure 6*a*. For the same geometry in the convection-dominated regime corresponding to $\mathrm{Ra} = 1{,}560$, stronger Rayleigh-Bénard cells develop over a number of heat sources, as shown in Figure 6*b*. The transition region occurs between $\mathrm{Ra} = 980$ and $\mathrm{Ra} = 1{,}560$ for this source length configuration, as shown in Figure 4. The radical change in Rayleigh-Bénard cell structure accounts for a sharper transition and high heat transfer rates in the convection-dominated regime, when compared to configurations of longer heat sources. With the larger and stronger convection cells present, heat transfer is improved. For configurations with source length and plenum height closer to a one-to-one ratio, the weak Rayleigh-Bénard cell structure that appears in the conduction-dominated

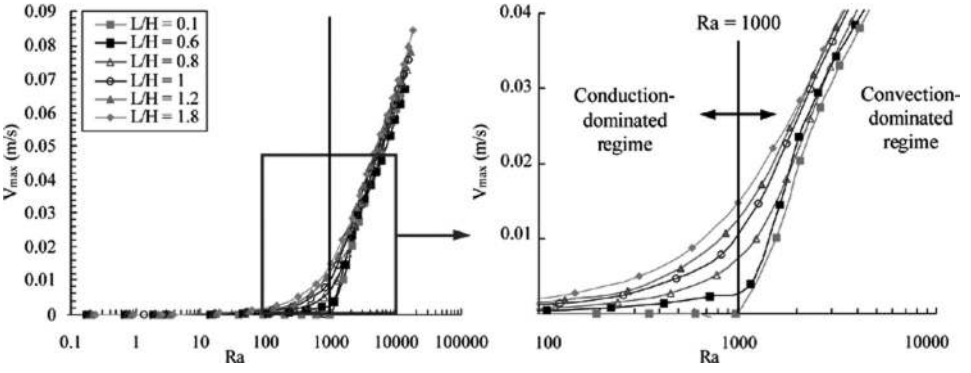

Figure 5. Maximum velocity versus Rayleigh number for various source lengths, L, while keeping the source spacing and source length equivalent ($S = L$).

regime remains similar in the convection-dominated regime. Without an abrupt change in Rayleigh-Bénard cell structure, the heat transfer rates are significantly lower than for the $L = 0.1\,H$ configuration. With respect to modeling these flows, it is noteworthy that the domain size requirement increases greatly following the transition to the convection-dominated regime. The domain shown in Figure 6*a* is sufficient to ensure domain size-independent solutions in the conduction-dominated regime. Following the transition, however, only two cells fill this same area. To avoid artificial forcing of the solution to specific cell patterns/wavelengths, a sufficiently large computational domain must be used for all simulations near the transition region (as shown in Figure 6*b*, inset).

For the case where $L = 0.4\,H$, bifurcations were observed for Rayleigh numbers beyond 2,900, which occurs well within the convection-dominated regime. Depending on the size of the domain, the structure of the Rayleigh-Bénard cells changes and cells develop over multiple heat sources. Figure 7 illustrates the bifurcation observed for this configuration where the Ra = 3,660 and the number of heat sources in the domain is 10, 15, and 20 in Figures 7*a*, 7*b*, and 7*c*, respectively. It is important to note that these solutions are not artifacts of the computational domain.

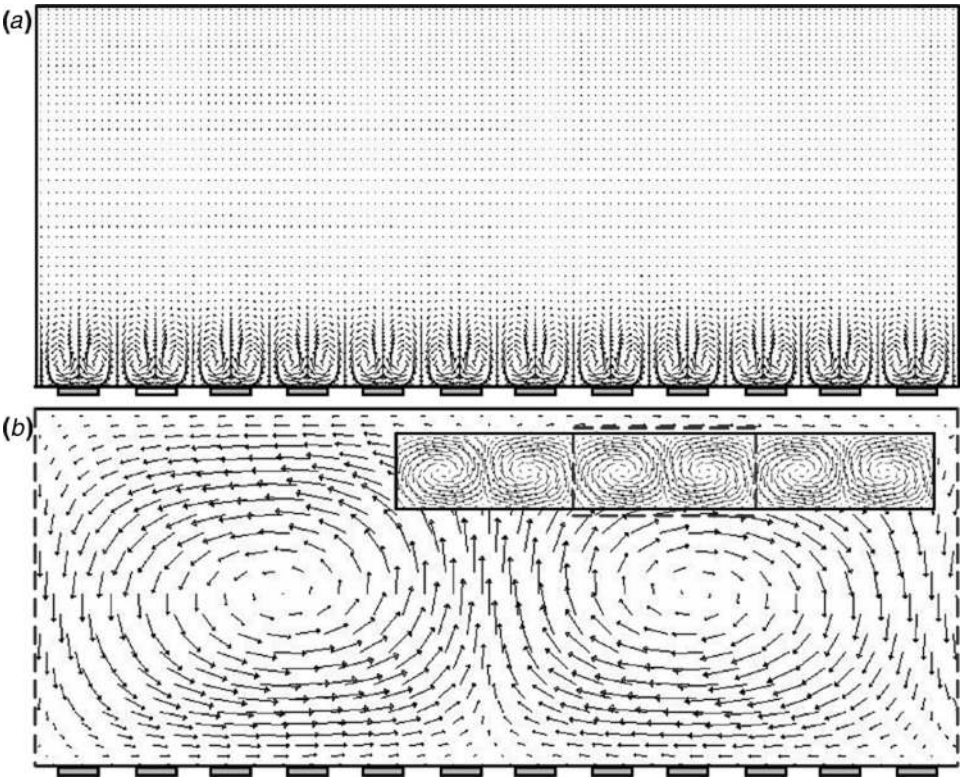

Figure 6. Velocity vectors for the $L = 0.1\,H$ configuration showing the change in Rayleigh-Bénard cell structure and domain size requirements at the transition region: (*a*) Ra = 980; (*b*) Ra = 1,560. Left and right edges are dashed to indicate that these results are part of a larger domain, shown in the inset.

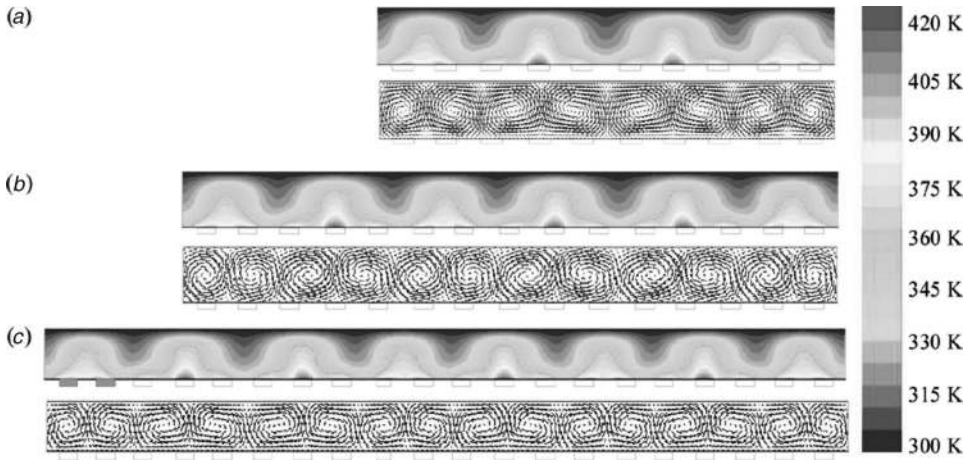

Figure 7. Temperature contours and velocity vectors for the $L = 0.4\,H$ configuration showing bifurcation of Rayleigh-Bénard cell patterns: (*a*) domain with 10 heat sources; (*b*) domain with 15 heat sources; (*c*) domain with 20 heat sources.

The nonuniqueness of the solution is an inherent physical and numerical feature of Rayleigh-Bénard flows [24]. Heat transfer coefficients and maximum velocities do not vary significantly for the solutions obtained at this Rayleigh number in Figures 7*a*, 7*b*, and 7*c*. It is important to note that other solutions generating different flow patterns may be possible, depending on physical or numerical perturbations [24].

For the case where $L = 0.6\,H$, a bifurcation associated with a regime change is observed for $5{,}800 < \mathrm{Ra} < 8{,}100$, well within the convection-dominated regime. At $\mathrm{Ra} = 5{,}800$, a thermal plume develops over pairs of heat sources, whereas at $\mathrm{Ra} = 8{,}100$, a thermal plume develops over each heat source. This bifurcation is accompanied by an abrupt decline in heat transfer, as shown in Figure 8. This is

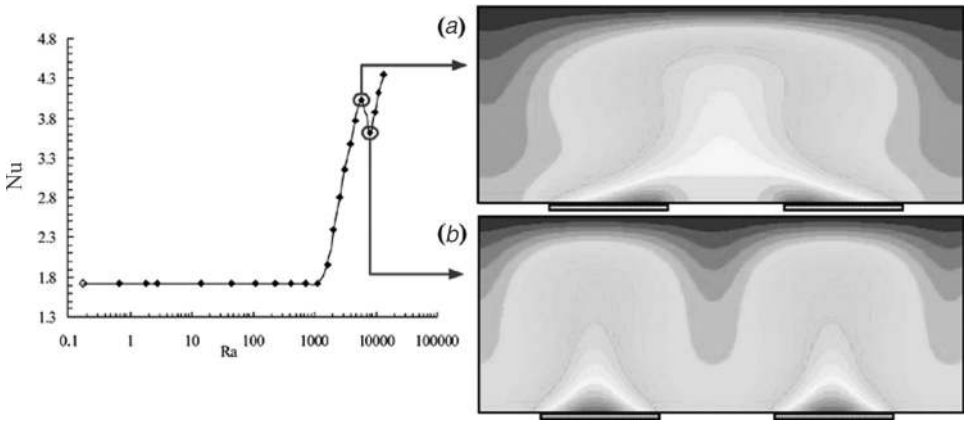

Figure 8. Average Nusselt number versus Rayleigh number for $L = 0.6\,H$ showing the bifurcation of cell structure in the convection-dominated regime corresponding to the abrupt change in Nusselt number from 4.0 to 3.6: (*a*) $\mathrm{Ra} = 5{,}800$; (*b*) $\mathrm{Ra} = 8{,}100$.

in contrast to the coalescence of cells observed at transition for smaller source lengths, and which resulted in an increased rate of heat transfer, as shown in Figure 6. The average Nusselt number decreases from 4.0 to 3.6 when Ra changes from 5,800 to 8,100. The maximum velocity does not experience any abrupt changes in this Rayleigh number region, but the thermal plumes change from developing over a pair of heat sources at Ra = 5,800 to a plume developing over each heat source at Ra = 8,100, as shown in Figures 8*a* and 8*b*, respectively. Due to the nonlinearity of the Rayleigh-Bénard problem, degeneracy of this nature is possible and similar phenomena have been observed in other natural-convection flow situations [24–26].

Nikfetrat et al. [24] investigated the machine and mesh sensitivity and the effect of initial perturbations on the onset and development of natural-convection in fluids. They noted that the problem is characterized by nonunique solutions, and that the specific numerical realization that is obtained depends on numerical noise, which causes uncontrolled perturbations. They suggested that when the perturbation applied to the actual physical process is well characterized, a similar numerical perturbation should be applied to the simulation to match this situation. Bahloul et al. [25] also observed Rayleigh-Bénard bifurcation in the numerical solution of natural convection in a vertical porous slot heated from below. D'Orazio et al. [26] presented a two-dimensional natural-convection problem in a tall vertical rectangular enclosure heated from below and cooled from above. Bifurcations were observed in the convection-dominated regime, which resulted in both smooth and abrupt changes in Nusselt number. This work is the first report of bifurcations associated with discrete heat sources in a horizontal air plenum that lead to significant heat transfer reductions.

CONCLUSIONS

A numerical analysis of convection patterns associated with distributed heat sources in an enclosure was conducted. The use of periodic boundary conditions and the investigation of the effect of various geometric parameters and flow parameters has provided new insight on the parameters governing the onset of natural-convective flow and associated heat transfer for arrangements relevant to passive cooling for microelectronics. The following conclusions can be drawn from the results obtained from this investigation.

First, it was determined that the source spacing of $S = L$ provides effective convective heat transfer, and is used for the parametric simulations. The heat transfer rates increase as the spacing length between sources increases, but reach a ceiling for spacing lengths larger than $S = L$. Increasing the spacing beyond this length is of little interest for small-scale device design, as it would lead to redundant substrate cost, added weight, and added volume.

Second, the transition from the conduction-dominated regime to the convection-dominated regime occurs within a range of values, which is in contrast to the well-known case of a uniformly heated bottom surface with side-wall confinement. The transition region is recognized as the elbow region of the average Nusselt number versus Rayleigh number. For source lengths ranging from $L = 0.1\,H$ to $L = 1.8\,H$, the transition region occurs at Rayleigh numbers ranging from 500 to 2,000. The range of Rayleigh numbers at which transition takes place decreases as

the source length increases. A corresponding transition region occurs in the plot of maximum velocity versus Rayleigh number.

As the source length decreases, the transition region becomes sharper, approaching the familiar bottom wall heating solution [21]. The transition elbow region becomes smoother and occurs at lower Rayleigh numbers as the source length increases. In the conduction-dominated regime, the average Nusselt number decreases as the source length increases. The maximum velocity increases at a faster rate as Rayleigh number increases for longer sources in the convection-dominated regime.

For shorter sources, the Rayleigh-Bénard cell structure changes at the transition region. In the convection-dominated regime, stronger cell pairs develop over a number of heat sources, replacing the weak and more numerous cells that appear in the conduction-dominated regime. The dramatic change in Rayleigh-Bénard cell size accounts for the sharp transition and high heat transfer rates in the convection-dominated regime, when compared to configurations with longer heat sources.

Bifurcations in cell structure were observed for the configuration of $L = 0.4\,H$ for Rayleigh numbers beyond 2,900; however, these solutions did not result in changes in the heat transfer rates. At a configuration of $L = 0.6\,H$, a bifurcation associated with a regime change was observed between Rayleigh numbers 5,800 and 8,100. The Rayleigh-Bénard cell structure changed from cell pairs developing over heat source pairs at $\mathrm{Ra} = 5{,}800$ to cell pairs developing over each individual heat source at $\mathrm{Ra} = 8{,}100$. This bifurcation was accompanied by an abrupt decrease in heat transfer, in line with recent work by D'Orazio et al. [26]. The insight this article has provided on the bifurcations associated with this particular geometry are of significant design considerations, since operating at a Rayleigh number at or beyond this transition does not provide any heat transfer improvements. All solutions were equally valid considering the nonlinearity of the Rayleigh-Bénard problem and its high sensitivity to perturbations, both physical and numerical [24].

REFERENCES

1. M. Arik, Thermal Modeling and Performance of High Heat Flux SOP Packages, *IEEE Trans. Advanced Packaging*, vol. 27, no. 2, pp. 398–412, 2004.
2. M. Krishnan, N. Agrawal, M. A. Burns, and V. M. Ugaz, Reactions and Fluidics in Miniaturized Natural Convection Systems, *Anal. Chem.*, vol. 76, no. 21, pp. 6254–6265, 2004.
3. S. J. Lee, A. Chang-Chien, S. W. Cha, R. O'Hayre, Y. I. Park, Y. Saito, and F. B. Prinz, Design and Fabrication of a Micro Fuel Cell Array with "Flip-Flop" Interconnection, *J. Power Sources*, vol. 112, pp. 410–418, 2002.
4. S. Litster, J. G. Pharoah, G. McLean, and N. Djilali, Computational Analysis of Heat and Mass Transfer in a Micro-structured PEMFC Cathode, *J. Power Sources*, in Press, 2005.
5. S. Rosentblat and G. A. Tanaka, Modulation of Thermal Convection Instability, *Phys. Fluids*, vol. 14, no. 7, pp. 1319–1322, 1971.
6. I. Catton, The Effect of Insulating Vertical Walls on the Onset of Motion in a Fluid Heated from Below, *Int. J. Heat Mass Transfer*, vol. 15, pp. 665–672, 1972.
7. J. Mantle, M. Kazmierczak, and B. Hiawy, The Effect of Temperature Modulation on Natural Convection in a Horizontal Layer Heated from Below: High-Rayleigh-Number Experiments, *J. Heat Transfer*, vol. 116, pp. 614–620, 1994.

8. C. Y. Soong, P. Y. Tzeng, and C. D. Hsieh, Numerical Study of Bottom-Wall Temperature Modulation Effects on Thermal Instability and Oscillatory Cellular Convection in a Rectangular Enclosure, *Int. J. Heat Mass Transfer*, vol. 44, pp. 3855–3868, 2001.
9. I. Martorell, J. Herrero, and F. X. Grau, Natural Convection from Narrow Horizontal Plates at Moderate Rayleigh Numbers, *Int. J. Heat Mass Transfer*, vol. 46, pp. 2389–2402, 2003.
10. F. P. Incropera, J. S. Kerby, D. F. Moffatt, and S. Ramadhyani, Convection Heat Transfer from Discrete Heat Sources in a Rectangular Channel, *Int. J. Heat Mass Transfer*, vol. 29, no. 7, pp. 1051–1058, 1986.
11. T. J. Heindel, S. Ramadhyani, and F. P. Incropera, Conjugate Natural Convection from an Array of Discrete Heat Sources; Part 1—Two- and Three-Dimensional Model Validation, *Int. J. Heat Fluid Flow*, vol. 16, no. 6, pp. 501–510, 1995.
12. T. J. Heindel, F. P. Incropera, and S. Ramadhyani, Conjugate Natural Convection from an Array of Discrete Heat Sources: Part 2—A Numerical Parametric Study, *Int. J. Heat Fluid Flow*, vol. 16, no. 6, pp. 511–518, 1995.
13. T. J. Heindel, F. P. Incropera, and S. Ramadhyani, Enhancement of Natural Convection Heat Transfer from an Array of Discrete Heat Sources, *Int. J. Heat Mass Transfer*, vol. 39, no. 3, pp. 479–490, 1996.
14. A. Ortega and B. S. Lall, Natural Convection Air Cooling of a Discrete Source on a Conducting Board in a Shallow Horizontal Enclosure, *Twelfth IEEE SEMI-THERM Symp.*, pp. 201–213, 1996.
15. Q. H. Deng, G. F. Tang, and Y. Li, Interaction between Discrete Heat Sources in Horizontal Natural Convection Enclosures, *Int. J. Heat Mass Transfer*, vol. 45, pp. 5117–5132, 2002.
16. S. K. W. Tou and X. F. Zhang, Three-Dimensional Numerical Simulation of Natural Convection in an Inclined Liquid-Filled Enclosure with an Array of Discrete Heaters, *Int. J. Heat Mass Transfer*, vol. 46, pp. 127–138, 2003.
17. J. H. Bae and J. M. Hyun, Time Dependent Buoyant Convection in an Enclosure with Discrete Heat Sources, *Int. J. Thermal Sci.*, vol. 43, pp. 3–11, 2004.
18. A. K. da Silva, G. Lorenzini, and A. Bejan, Distribution of Heat Sources in Vertical Open Channels with Natural Convection, *Int. J. Heat Mass Transfer*, vol. 48, pp. 1462–1469, 2005.
19. A. K. da Silva, S. Lorente, and A. Bejan, Optimal Distribution of Discrete Heat Sources on a Wall with Natural Convection, *Int. J. Heat Mass Transfer*, vol. 47, pp. 203–214, 2004.
20. C. P. Tso, L. F. Jin, S. K. W. Tou, and X. F. Zhang, Flow Pattern in Natural Convection Cooling from an Array of Discrete Heat Sources in a Rectangular Cavity at Various Orientations, *Int. J. Heat Mass Transfer*, vol. 47, pp. 4061–4073, 2004.
21. E. Papanicolaou and S. Gopalakrishna, Natural Convection in Shallow Horizontal Air Layers Encountered in Electronic Cooling, *J. Electronic Packaging*, vol. 117, pp. 307–316, 1995.
22. Fluent, Inc., Lebanon, NH, *Fluent 6.1.22*, 2003.
23. F. P. Incropera and D. P. De Witt, *Fundamentals of Heat and Mass Transfer*, p. 559, Wiley, New York, 1990.
24. K. Nikfetrat, N. Djilali, and S. Dost, Accuracy and Nonuniqueness Aspects of Numerical Solutions of Some Natural Convection Problems, *Appl. Math. Modelling*, vol. 20, pp. 371–378, 1995.
25. A. Bahloul, L. Kalla, R. Bennacer, H. Beji, and P. Vasseur, Natural Convection in a Vertical Porous Slot Heated from Below and with Horizontal Concentration Gradients, *Int. J. Thermal Sci.*, vol. 43, pp. 653–663, 2004.
26. M. C. D'Orazio, C. Cianfrini, and M. Corione, Rayleigh-Bénard Convection in Tall Rectangular Enclosures, *Int. J. Thermal Sci.*, vol. 43, pp. 135–144, 2004.